Conductivity of 2-D Ag Quantum Dot Arrays: Computational Study of the Role of Size and Packing Disorder at Low Temperatures

F. Remacle,[†,‡] K. C. Beverly,[§] J. R. Heath,[§] and R. D. Levine*[,†,§]

The Fritz Haber Research Center for Molecular Dynamics, The Hebrew University of Jerusalem, Jerusalem 91904, Israel, Département de Chimie, B6c, Université de Liège, B4000 Liège, Belgium, The California NanoSystems Institute and the Department of Chemistry and Biochemistry, The University of California Los Angeles, Los Angeles, California 90095

Received: October 24, 2001; In Final Form: February 4, 2002

The temperature dependence of the coherent DC conductivity of an Ag quantum dot (QD) monolayer has been computed allowing for size fluctuations of the QDs as well as for packing disorder. The computation uses a scattering formalism with an electron exchange coupling for adjacent QDs. The strength of this coupling can be tuned by compression of the array, and the same coupling is used as previously determined from second harmonic generation spectroscopy of such monolayers. To agree with the experimental results, the computations center attention on the regime of not fully compressed arrays, when the exchange coupling does not fully mask the role of disorder. At very low disorder and/or at higher compressions, the computations show a phase transition to a fully delocalized conducting regime. At very low temperatures, the computed conductivity increases with temperature as $\exp(-2(E_0/kT)^{1/2})$. The characteristic energy E_0 is found to be a measure of the effective coupling of next-nearest neighbors, suggesting that conduction occurs by variable range charge hopping or, in the language of electron transfer, by super-exchange. At higher temperatures, there is a crossover to an activated regime, $\exp(-(E_a/kT))$, where the activation energy E_a is shown to be a measure of the mean excess energy of the moving charges. The transition temperature to activated conduction scales with the extent of disorder. The increase of conductivity with temperature is interpreted as reflecting a gap in the density of conducting states for energies just above the ground electronic state of the array.

1. Introduction

A physical understanding of the process of charge transport is required for most intended applications of nanoscale and molecular electronic devices.[1] There is therefore current experimental work directed at characterizing the collective response and the transport properties of chemically assembled arrays of metallic quantum dots (QDs).[2] The response can be a collective one because the individual QDs are coupled by electron exchange. This coupling is a rapidly decreasing function of the interdot separation, and so the coupling is sensitive to the compression of the array and to any packing disorder. The effective coupling between the QDs is also modulated by any variation in the energies of the exchanged electrons on the dots. The more nearly similar the dots are, the more the electron exchange coupling is able to establish a collective behavior. As is well understood,[3] the energy of the higher-most electron in a metallic dot is governed by its size, and so a collective behavior of an array requires as narrow a size distribution of the individual dots as possible and/or as tight a coupling as possible.

In this paper, we provide a direct quantum mechanical computational test of these ideas. What enables us to provide a detailed view is the introduction of two additional experimental variables. One is the temperature of the array, which allows for a fined energy resolution beyond what was previously achievable. The other variable is the electrical potential gradient across the array. By changing this gradient, we can independently gauge the role of the different physical parameters that characterize the isolated array. We compare our computational results with the experimental data of Beverly et al.[4] The qualitative and quantitative similarity between the experimental and computational results appears to us to lend support to the physical picture that we will offer. We shall however also seek to delineate the limitations of the theoretical model.

The experimental results that we aim to compare with are described in detail elsewhere.[4] They are for arrays of hexagonally ordered, dodecanthiol-capped 70 Å diameter Ag QD monolayer films. The size distribution of the dots is narrow and tunable over the range from 14 to 6%, and monolayer films bridge a 5 μm gap separating two electrodes. A potential gradient of 0.1 V is applied across the array. For a compressed film 5 μm wide, there are roughly 700 dots across, and so the potential drop per dot is about 1.4×10^{-4} V/particle, a parameter that enters into our model. The Hamiltonian that we use is the same as that we employed in several previous computations on these types of systems. One such calculation included the effect of compression (decreasing interparticle separation distance) on the second harmonic generation response of the array.[5] That computation allowed us to set the strength and range of the electron exchange coupling of the dots. Then the same parameters, augmented by the charging energy[6] per dot, were shown to reproduce the frequency dependent dielectric constant of the array, as well as the variation of this frequency with compression. This included the nonmetal to metal transition in

* To whom correspondence should be addressed. E-mail: rafi@fh.huji.ac.il. Fax: 972-2-6513742.
† The Hebrew University of Jerusalem.
‡ Université de Liège.
§ The University of California Los Angeles.

10.1021/jp013937a CCC: $22.00
Published on Web 03/30/2002

the collective response. The same Hamiltonian could then represent the local density of states as probed by STM spectroscopy [7] including the effects of a broad size distribution of the dots. Most recently, the idea [8] of domain localized states that are characteristic of lower compressions could be validated by measurements of the surface potential.[9]

To compute the conductivity of the array, we shall use the scattering formulation as pioneered by Landauer[10] and extensively discussed in the literature.[11] We emphasize that this implies that the charge transport in a small, well ordered, domain is coherent: there is no scattering of the electrons by phonons or by packing imperfections. In terms of solid-state physics,[10,11] this means that we are using a, so-called, mesoscopic approach where the coherence length is longer than the size of the sample. Such an approach has been used to compute the conductivity of single molecules.[12−14] It is a valid question to ask just how valid is the assumption that a single domain of many dots behaves like a single molecule. The approach that we use is consistent with such a picture, and so far, it has correctly reproduced the spectroscopic response[5] as well as other collective behavior of small, orderly packed arrays of quantum dots, including the frequency dependence of the dielectric constant.[6] We can and have explored the effect of change of phase of the electron because of elastic collisions,[15] but we have not allowed for any dissipation. Our approach is therefore complementary to a scattering of the electron by different dots. The other limitation is that we do not explicitly include the effects of Coulomb blocking. The reason is that we carry out computations for finite size domains of hexagonal unit cell. Explicitly allowing for Coulombic repulsion of electrons, which is a two electron correlation effect, requires a basis size which is completely prohibitive. (One needs to allow for at least four states per dot, so that, for N dots there are 4^N states of the array. Not all of them are doublet states, but even for a minute array of 19 dots, there are nearly 3 billion doublet states.[6] The ground state is a doublet because the hexagonal array has an odd number of dots.) Fortunately, the experiment is on our side. To have a measurable 0-bias conductance at low-temperatures, one needs to use a fairly compressed array; that is, one that is metallic (in the sense that its resistance is decreasing with temperature), or nearly metallic, at room temperature.[4] For the case of a metallic array, this means that we are in the regime where the single particle charging energy, I, (i.e., $I = e^2/C$, where C is the capacitance of an isolated particle) is smaller than the exchange coupling strength. So we are in a different regime than that appropriate to metallic films (see ref 16 for example). In terms of the electronic states, this means that the covalent and ionic states of the array are already mixed. We have verified this through computations on the smallest hexagonal array. Our earlier computations have established that the tight-binding Hamiltonian that we use provides a realistic description in this stronger coupling regime.

An important variable in our computations is the temperature. Typically, computations on conductivity of single molecules invoke only the effect of temperature on the distribution of electrons in the electrodes.[11−13] This is because the electronic orbitals of a single, not too large, molecule are spaced sufficiently apart that the excited states cannot be thermally populated. This is definitely not the case for our array, and for us, the primary role of temperature that we see is due to higher and higher electronic states of the array becoming available as we increase the temperature.

2. Conductivity

In the scattering formalism,[11,12,14] the current flowing across an array placed between two electrodes is usually expressed by

$$i = \frac{e}{2\pi\hbar}\int \mathrm{d}E\; T(E)[f_{\mathrm{l}}(E) - f_{\mathrm{r}}(E)] \cong \frac{2e^2V}{h}\int \mathrm{d}E\; T(E)\,[-\partial f/\partial E] \quad (1)$$

Here, $f_{\mathrm{l}}(E)$ and $f_{\mathrm{r}}(E)$ are the Fermi−Dirac occupation probabilities of the left and right electrodes and $T(E)$ is the transmission of the array and is the output of the scattering computations. The two electrodes are at a different electrochemical potential. In the linear regime, one uses a first-order Taylor expansion of the Fermi−Dirac occupation probabilities, whose Fermi levels differ by the voltage V, $f_{\mathrm{l}}(E) - f_{\mathrm{r}}(E) \cong -eV(\partial f/\partial E)$, to bring the voltage V difference explicitly out. The factor 2 is from the two spin directions. When the voltage drop per site (the term eV_{k} of eq 9 below) is low, the computed transmission is independent of the voltage. At higher field gradients, the computed transmission function is, by itself, a function of the voltage as discussed in connection with eq 9 and seen experimentally in studies of the surface potential.[9] At lower temperatures, and if the two electrodes are of the same material, the energy weighting factor of the electrodes is essentially a delta function at the Fermi energy of the electrodes

$$-\partial f/\partial E \xrightarrow{T\to 0} \delta(E - E_{\mathrm{F}})$$

Then one has, in the linear regime

$$i = \frac{2e^2V}{h}T(E_{\mathrm{F}}) \quad (2)$$

or, if there is more than one possible initial and final state

$$i = \frac{2e^2V}{h}\sum\nolimits_n T_n(E_{\mathrm{F}}) \quad (3)$$

There can be more than one final state, and the sum over final states is done at the level of the scattering amplitude, as is discussed below.

To perform a thermal average of expression 3 for the current, we need to specify the initial states in detail. This is very similar to what is done in scattering theory of composite particles.[17] In the present problem, there is the initial thermal energy distribution in the electrodes as well as the distribution of electronic states of the array. A key point for us is that higher electronic states of the array can be readily thermally accessed and so must be included in the thermal averaging. This is quite analogous to scattering calculations on molecular systems where one needs both a thermal average on the kinetic energy of the relative motion (the equivalent of the thermal energy spread in the electrodes) and a separate thermal average on the internal states of the colliding molecules. It may not be immediately obvious that these two averages can be performed independently. However, this is a well-known result of a canonical average; a result that is most familiar in the form that, when the energy is a sum of terms, the partition function is a product of terms. In scattering theory, the two averages can be easily performed because the initial energy, E_{n}, is a sum of the energy in the electrode and the energy of the internal electronic state of the array. Hence, using i to enumerate the internal electronic states of the array, the expression for the current, after thermal averaging for the electrodes, is

$$i = \frac{2e^2V}{h}\sum_i \langle n_i\rangle\langle T_i(E)\rangle \quad (4)$$

where $\langle n_i \rangle$ is the thermal occupancy of the ith electronic state of the array and $\langle T_i(E) \rangle$ is the result of averaging over the electrodes, for a given electronic state of the array

$$\langle T_i(E) \rangle \equiv \int \mathrm{d}E\, T_i(E)[-\partial f/\partial E] \tag{5}$$

The transmission of the array is computed as usual in scattering theory

$$T_i(E) = \sum_j |\sum_{j'} T^i_{j,j'}|^2, \qquad T^i_{j,j'} = \langle j|VG_iV|j' \rangle \tag{6}$$

The index i refers to the electronic states of the array, whereas j and j' are the initial and final states. V is the coupling of the right (and left) electrodes to the array, and we assume that the electrodes are not directly coupled. $G(E) \equiv (E - H)^{-1}$ is the Green's function for the complete problem, meaning the Hamiltonian H includes not only the array but also the coupling, V, of the electrodes to the array. Note that there can be more than one possible final state and that we add coherently all of the different scattering pathways starting from the same initial state.

3. The Electronic Problem

A representation of a small hexagonal array of 6 dots per side and 91 dots in all is shown as an insert Figure 1. We compute the conductivity between two opposite sides of such an array but with 55 dots per side. The number of dots connecting two such sides is roughly $(3)^{1/2}$ times the number of dots per side. We use j and j' to enumerate the dots on the two facing sides such that the voltage gradient favors a current flow from j to j'. We mimic the electrodes as the row of dots on the left and right side of the array. Expression 6 for the current can then be written as

$$i = \frac{2e^2V}{h}\sum_i \langle n_i \rangle \sum_j |\sum_{j'} \langle j|VG_iV|j' \rangle|^2 \cong \frac{2e^2V}{h}\sum_i \langle n_i \rangle \sum_j |\sum_{j'} \pi \langle j|V\delta(E_i - H)V|j' \rangle|^2 \tag{7}$$

The Hamiltonian for the array is the same tight binding approximation as we have used before.[18,19] It has terms representing the single electron energy on a given site and the exchange coupling between neighboring sites:

$$H_0 = \sum_k^N \alpha_k \sum_\sigma^2 a^\dagger_{k,\sigma} a_{k,\sigma} + \sum_{\substack{k,k' \\ \text{near neighbors}}}^N \beta_{k,k'} \sum_\sigma^2 a^\dagger_{k,\sigma} a_{k',\sigma} \tag{8}$$

The $a^\dagger$ and a in eq 8 are the creation and annihilation operators for an electron at a given site and with a given spin (σ = up or down). The sites need not have equal energies (IPs), and the variations in the site energies α_k are discussed below. N represents the number of dots in the array. β, the transfer integral, is the coupling which moves an electron from one orbital to another. Note that because of the spin labels an electron can only move into an empty spin−orbital, and this restricts conductivity to molecular orbitals which are empty or which contain at most one electron.

The Hamiltonian (8) is a one electron Hamiltonian, and it is diagonalized as an N by N symmetric matrix. Not included in this Hamiltonian are the two electron terms accounting for the Coulombic repulsion between electrons. First of all, it is missing the Coulombic repulsion between electrons of opposite spins on the same site. These, so-called Hubbard terms,[20,21] give rise to the effects due to the charging energy. However, at the higher compressions that we are interested in, where the exchange coupling β is larger than the charging energy, as evident from the metallic behavior at room temperature, this neglect is realistic. Also not accounted for is the Coulomb repulsion between electrons on different sites. Such two-electron terms are included in the more complete PPP-type (Pariser, Parr, Pople) Hamiltonian[22] that we have used. For a hexagonal array of seven dots, it is computationally tractable to have both types of terms. We report below that, for the compression range relevant to the conductivity experiments,[4] the role of these terms is small, although they are important at lower compressions (larger interparticle separation distances). In those cases, however, the measured conductivity is very low.

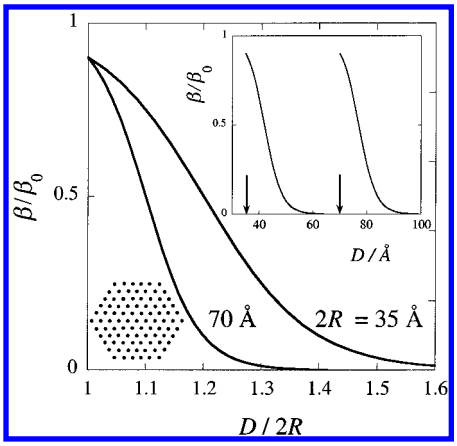

Figure 1. Exchange coupling β vs the scaled lattice spacing $D/2R$ for a hexagonal array. D is the spacing of adjacent dots, and $2R$ is the diameter of a dot. The dependence of β on $D/2R$ is shown for both small dots, $2R = 35$ Å, as used in our earlier computations, and for the larger dots, $2R = 70$ Å, used in the conductivity experiments. The insert shows the dependence of the exchange coupling β on the physical lattice spacing D so as to emphasize that for either set of dots the decline of β with distance between the dots is the same. The arrow indicates the diameter of the dot. See text for more details. The inset shows a small hexagonal array of six dots per side. The quantum mechanical computations reported below were carried out for a hexagonal array of 55 dots per side and 8911 dots in all.

In the Hamiltonian (8), α and β carry labels of the sites because the sites are not necessarily equivalent. This is due to the fluctuations in size of the dots and, in the case of the transfer integral β, also due to packing disorder. Taking the case of the site energies first, the valence orbital of a metallic dot is similar to the orbital of a particle in a spherical box of radius R. If the potential outside is infinite, the energy can be readily computed analytically and scales as R^{-2}. The radius of the dot determines therefore the energy of the highest occupied orbital and also the charging energy. We are discussing larger dots (of mean diameter of 70 Å) so that the charging energy is low (about 0.1 eV). At intermediate or higher compressions where the exchange coupling is already larger than the charging energy, the role of the charging energy can therefore be neglected. Fluctuations in the size of the dots imply fluctuations in both the energy of the highest occupied orbital of the dot, $|\delta\alpha| = \alpha 2|\delta R/R|$ and in the interdot coupling, as discussed in eq 10 below. The fractional fluctuations are roughly the same because both energies decrease with increasing size of the dot. In the computations, we draw a magnitude of R from the experimentally achieved narrow size distribution [4] and use it to compute the value of the energy parameters of that dot.

We also include a systematic variation of the site energies, due to the imposed external electrical potential. Thus, the complete expression for the energy of site k is

$$\alpha_k = \alpha_0(1 + \delta\alpha_k) + eV_k \qquad (9)$$

$\Delta\alpha \equiv \alpha_0\,\delta\alpha$ is the range of variation in the site energies because of the fluctuations in the size of the dots. $\delta\alpha_k$ is the fractional range of variation in the site energies, $\delta\alpha$, multiplied by a random number between -1 and 1 so that the site energy of the kth dot in the array is $\alpha_0(1 + \delta\alpha_k)$. The last term in eq 9 is due to the external electrical potential. V_k is the external potential at the position of the kth dot, computed from the geometry of the array. Explicitly, if the potential bias of 0.1 V is applied at the electrodes and there are 100 dots that span the gap, then the potential at the 50th dot will be 0.05V.

In the absence of an external potential, the energies of different dots are uncorrelated. Once a potential is applied, there is a systematic contribution to the site energy. Adjacent dots are correlated if they are oriented in the direction of the potential gradient, whereas they remain uncorrelated otherwise. When the applied voltage gradient is sufficiently large, the systematic monotonic variation in the site energies can compete with the fluctuations. We confirmed this theoretical prediction by comparing with an experimental measurement of the surface potential (SP) under conditions of increasing the voltage drop per particle. Thereby, one can observe[9] a transition from a domain localized state where there are "islands" of higher SP to stripe-like regions where the stripes are directed along the gradient. Such transitions require however a large enough potential gradient that the conductivity is no longer linear in the applied voltage. Most of the computations that we shall report are in the linear regime where the role of the third term in the equation is more limited.

The early quantitative results on the role of compression for an Ag QD array[5] were fitted using an exchange coupling of the functional form

$$\beta = (\beta_0/2)(1 + \tanh((D_0 - D)/4RL)) \xrightarrow{D > 2R} \beta_0 \exp(D_0/2RL)\exp(-D/2RL) \qquad (10)$$

where R is the radius of the metal core of the dot and D is the separation between the centers of adjacent dots, i.e., the lattice constant. For those dots, which were relatively small, $\langle 2R\rangle = 35$ Å, the fit to the experimental second harmonic generation efficiency as a function of $D/2R$ gave $1/2L = 5.5$ and $\beta_0 = 0.5$ eV. The range of strong coupling was determined by the value $D_0/2R = 1.2$. This very same coupling was able to the reproduce the experimentally measured effect of lattice compression on the frequency dependent complex dielectric function[6,23] and also of local properties such as the variations of the surface potential across the array[9] or the local density of states as probed by STM spectroscopy.[7,24] The same functional for the exchange coupling is used in this paper. However, the experimental results were obtained for arrays of dots of a number of different sizes. The most extensive data set (and the tightest size distributions) are for dots where $\langle 2R\rangle = 70$ Å. The exchange coupling is determined by the overlap of wave functions on adjacent dots and is therefore expected to scale with the distance D between the dots as $\exp(-\kappa D)$ where the length scale $1/\kappa$ is determined by the energy of the highest orbital and the effective mass of the electron in that orbital.[25] Therefore, we expect $2RL$ to be roughly independent of the size of the dot, and so we here used $1/2L = 11$. Also, we expect that on contact, i.e., for $D/2R = 1$, the strength of the coupling is roughly the same for all sizes, and this requires setting $D_0/2R = 1.1$ for the larger dots. The strength of the exchange coupling is shown both vs D and vs $D/2R$ in Figure 1. The plot serves to emphasize that because $\langle R\rangle$ is now double in value, the coupling in the present case is a faster falling function of $D/2R$. Even so, the lower value of the charging energy for the dots of interest here means that, in the absence of size fluctuations, the onset of the Mott metal to non metal transition [21] occurs for arrays expanded beyond $D/2R = 1.3$.

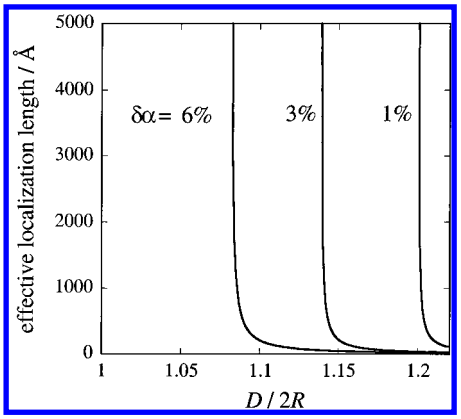

Figure 2. Transition to a delocalized state as the lattice is compressed for three values of the (fractional) lattice disorder $\delta\alpha$, as shown. The experimental results are for $\delta\alpha > 6\%$ and $1.1 < D/2R < 1.2$. The experimental results are therefore to the right of the transition to the delocalized state. See text for more details.

The conductivity of the array saturates when the exchange coupling is strong enough to bridge any local fluctuation of the site energies, that is as $D/2R \rightarrow 1$. In this region, the electronic wave function is fully delocalized. As the array is expanded past the point where $D/2R = D_0/2R$, one enters the domain localized regime [8] where the wave function is localized over a fraction of all of the dots. The more $D/2R$ exceeds $D_0/2R$, the weaker the coupling is and the more localized the wave function is, as shown in Figure 5 below. When the localization length scale is short, the conductivity is exponentially small and can no longer be experimentally measured as it falls outside of the dynamic range of a setup that is suitable for the range just below metallic behavior. An important implication of the faster falloff of the coupling of larger dots with $D/2R$ is that the range of lattice compressions where the conductivity is not exponentially small is a narrow one. Only a limited window in $D/2R$ can be experimentally probed. We note the obvious, namely, that the accessible range in $D/2R$ is small because R is large and that the physical spacing, $D - 2R$, between the dots can still be varied by quite a bit, say from 7 to 15−20 Å. However, unlike the earlier experiments that used smaller dots, we are here interested in changes that occur as the array is compressed over a narrow range in $D/2R$.

The strength of the exchange coupling is measured with respect to the variation in the energies of adjacent sites. Therefore, the effective coupling is $\beta/\Delta\alpha$. Perturbation theory suggests that the change in the wave function n sites away from a given site is, in leading order, $(\beta/\Delta\alpha)^n$. Defining the "localization length" ξ by the electronic density decreasing with the distance r as $\exp(-r/\xi) = \exp(-nD/\xi) = (\exp(-D/\xi))^n$, we can define an effective localization length in terms of the effective coupling strength $\exp(-D/\xi) \equiv (\beta/\Delta\alpha)^2$. This effective localization length is plotted vs $D/2R$ in Figure 2. The divergence of this simple measure is at the Anderson-like[21,26] transition to a delocalized state. We have earlier presented evidence that such

a transition can take place, for smaller dots.[18] Here the dots are larger and so, for a given disorder, the lattice needs to be compressed to smaller values of $D/2R$ for the transition to take place. Below we shall present computational results for the shape of the wave function, and these will verify the semiquantitative arguments above.

Figure 2 suggests that for any reasonable coupling strength, depending on the extent of disorder, one can be either to the left of the transition, where the electronic states are fully delocalized, or to the right of it where the states are either domain localized if $\beta/\Delta\alpha$ is just below unity or fully localized if the size fluctuations are wider. The last case, $(\beta/\Delta\alpha) < 1$, is not easy to probe because of the limited conductivity that characterizes such arrays. Of course, just to the right of the transition, the conductivity will exponentially decrease with increasing disorder, but this decrease is much more moderate than when one is well to the right of the transition.

The functional form of the exchange coupling (eq 10) shows that it has local variations for at least two reasons. First, fluctuations in the size (R) of the dots imply that β will vary. Next, small packing disorder, small enough not to disturb the hexagonal arrangement of the dots, can also lead to fluctuations in the exchange coupling. The physical array can also have packing fault lines and other structural irregularities that lead to a polycrystalline order of only limited hexagonally packed domain sizes. The effects of such faults are harder to incorporate. However, if these are extensive, then the assumption of a coherent array response may no longer be valid.

In the computations, we simulate the experimental conditions of arrays of dots with a narrow (3−14%) size distribution so that the fluctuations in the site energies and coupling are small to moderate in magnitude. This is an important point because, for wider fluctuations, the gap in the density of conducting states, a gap that in our interpretation results in the interesting behavior of the conductivity at low temperatures, gradually closes and the effects at very low temperatures, that we will discuss, wash out.

Before closing the discussion of the electronic structure, we reiterate that the computations of the conductivity for the large arrays with finite disorder were carried out without incorporating the quantitative effects due to charging energy. One expects that, given the steep drop of the exchange coupling as the lattice decompresses, cf. Figure 1, the charging effects become qualitatively important for $D/2R = 1.3$. Figure 3 provides the computational evidence. It shows the excitation spectrum above the ground state of a hexagonal array of seven dots including explicit Coulomb repulsion. These are the same type of computations as we reported earlier[6,7] but for the lower value (0.1 eV) of the charging energy and the shorter range in $D/2R$ exchange coupling that are appropriate for larger dots. The computations shown are for a disorder of 5%, which is just below the current experimental range. For a higher amount of disorder, the results in the panels as shown are even more similar to each other. The three panels are for (a) including only the on-site Coulomb repulsion, the, so-called, Hubbard or charging energy terms and (b) including also Coulomb repulsion between electrons on adjacent dots. The latter are the PPP or cross-capacitance terms. Panel c is the same results but for the one electron Hamiltonian (8). At the lower values of $D/2R$, the picture of the electronic states is very similar to the one electron results: There are disorder-induced domain localized states that only become truly delocalized at stronger coupling. What is shown in Figure 3 are the actual energies of the N electron states and not energies of one electron molecular orbitals. Therefore,

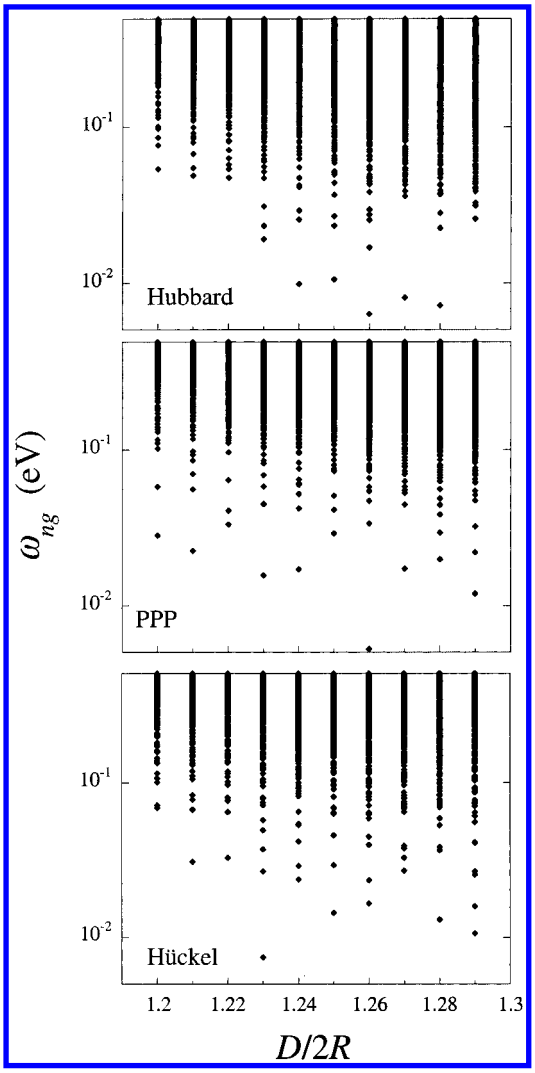

Figure 3. Energies of states above the Fermi energy computed in the Hubbard, PPP and, Hückel approximations for $\delta\alpha = 5\%$ vs $D/2R$ for a hexagonal array of seven dots. In the range of lattice compression relevant to the experiment, the role of charging energy and of cross Coulombic effects is qualitatively unimportant and quantitatively small. Note that the energies shown are those of N electron states and not those of individual molecular orbitals.

Figure 3 brings forward another point: the mixed domain localized states are more prevalent for energies immediately above the ground state. In a one electron picture, one would say that the mixed states are more common just above the Fermi energy (≡ the energy of the HOMO).

At very low disorder, and for the compression range of interest, say $D/2R < 1.25$, the picture of the distribution of states is different. With only charging energy included, the gap between covalent and ionic terms occurs already at lower values of $D/2R$, Figure 4. The opening of the gap is the onset of the celebrated Mott[21] insulating phase. For a Hubbard Hamiltonian, the onset of the transition as a function of compression is very sensitive to disorder. The gap is above $D/2R = 1.3$ even for 3% disorder, but it comes down to the accessible experimental range of compressions when the disorder falls below 2% as shown in Figure 4. When we also include the Coulombic cross terms, the gap opens up not quite as sharply and the metal to insulator transition occurs at higher value of $D/2R$. The PPP results are therefore more similar to the Hückel, one electron results than when only on-site charging effects are included. Even so, the results in Figure 4 suggest that experiments for dots with a very

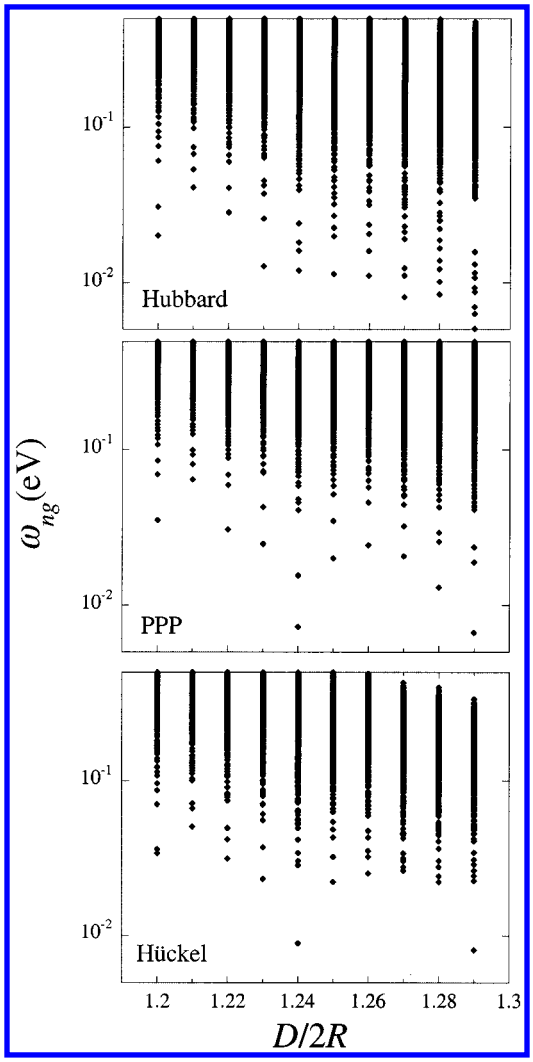

Figure 4. Energies of states above the Fermi energy computed in the Hubbard, PPP and, Hückel approximations for $\delta\alpha = 2\%$ vs $D/2R$ for a hexagonal array of seven dots. In the range of lattice compression relevant to the experiment and for, thus far, unattainably low disorder, the role of charging energy is qualitatively important as the covalent−ionic gap only closes at $D/2R \approx 1.27$. The transition can also be seen for the higher disorder as shown in Figure 3 but at a higher value of $D/2R$. To experimentally probe the Mott transition, one needs to either further decompress the lattice or to use dots of very narrow size distribution. Note that the cross Coulombic effects tend to smear out the Mott insulator−metal transition.

narrow size distribution are worthwhile, as is indicated by extrapolation of the experimental transport data as a function of decreasing particle size distribution width.[4] This point will be made again when we discuss the very low temperature dependence of the conductivity.

The changeover from a delocalized to a domain-localized to a strictly localized wave function is shown, for a large hexagonal array of 55 dots per side, in Figure 5. Shown is the weight of the HOMO along a line of sites diagonally connecting the two sides of the array. The steep transition as the disorder is increased is very evident. The results are for a Hückel one electron computation at $D/2R = 1.24$. The same transition is seen at all compressions. The exponential increase of the exchange coupling with compression means that the transition occurs at higher disorders when $D/2R$ is lower, cf. Figure 2.

Figure 5 reiterates the point that, for the range of experimental conditions of interest, we are just to the right (localized side) of the Anderson-like transition to a delocalized behavior.

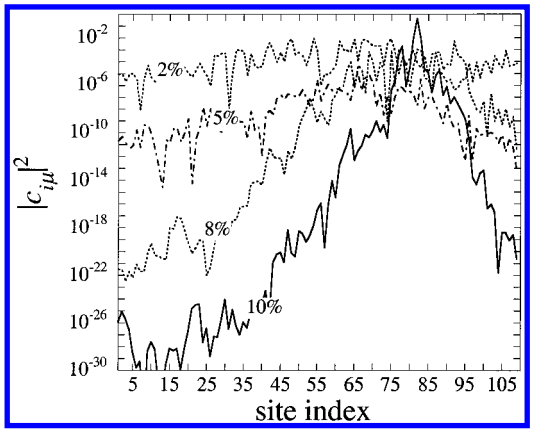

Figure 5. Quantum mechanical computations showing the decrease of the localization with decreasing disorder. Shown is the weight, on a logarithmic scale, of the HOMO on different dots along a diagonal line of an array of 55 dots for different values of disorder as shown. $D/2R = 1.24$. These computations use the same set of size fluctuations for all dots, and only the absolute range of the fluctuations is different. The particular dot that the wave function is localized at is determined by the accident of which dot has the lowest site energy. Note the exponential localization at high disorder, the domain localization at intermediate disorder, and the delocalization at a very low disorder. The higher $D/2R$ is, the wider the range of disorder for which the wave function is localized will be.

Similarly, Figures 3 and 4 show that we are to the left of the Mott metal to insulator transition. In other words, we are probing the intermediate coupling regime where neither of the limiting type models apply. The states of interest are neither delocalized nor strictly localized.

4. The Electronic Conductivity of the Array

Diagonalizing the Hamiltonian of the array, eq 8, gives rise to molecular orbitals that can accommodate up to two electrons of opposite spins. N electron states can be built by assigning electrons to molecular orbitals. Throughout the energies (temperatures) of interest here, most excited states correspond to just one electron being excited to a molecular orbital that, in the ground state, is unoccupied. One can therefore enumerate the excited states of the array in terms of the index of that excited molecular orbital that can be occupied at a finite temperature. The energies of these states begin with the, so-called, LUMO (lowest unoccupied molecular orbital), and we will index these orbitals by μ. For the Green's function, one therefore has the simple spectral representation

$$G_\mu(E) = |\mu\rangle(E - E_\mu)^{-1}\langle\mu| \tag{11}$$

This allows the scattering matrix element between two dots which are on opposite sides of the array, j and j', to be simply written as

$$\langle j|VG_\mu V|j'\rangle = \sum_k \sum_{k'} \langle j|V|k\rangle\langle k|G_\mu|k'\rangle\langle k'|V|j'\rangle$$
$$\cong i\pi \sum_k \sum_{k'} \langle j|V|k\rangle\langle k|\mu\rangle\delta(E - E_\mu)\langle\mu|k'\rangle\langle k'|V|j'\rangle \tag{12}$$

Here k and k' enumerate sites of the array that are coupled to the end sites j and j'. The coefficients $\langle k|\mu\rangle$ are the weight of the site state k in the molecular orbital μ and are determined by diagonalizing the Hamiltonian written as a matrix in the site basis. The averaging over temperature is carried out as in eq 7.

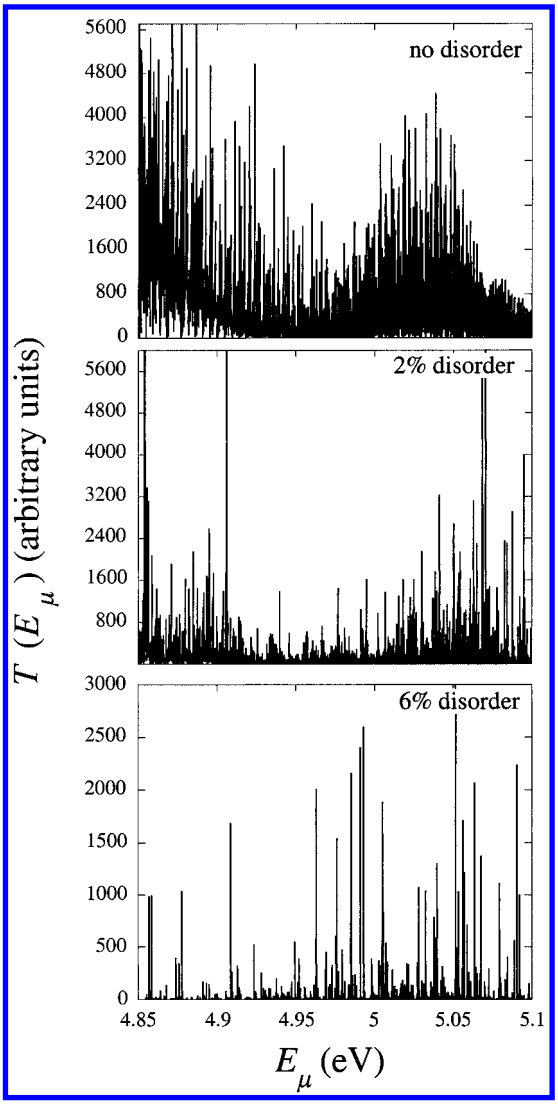

Figure 6. Quantum mechanical computations of the transmission of a hexagonal array of 8911 dots vs the energy E_μ of the molecular orbital. $D/2R = 1.21$.Shown for no disorder, low disorder and realistic disorder, as indicated on the panels. The plot is centered around the energy of the LUMO, but only the unoccupied molecular orbitals are conducting. This plot emphasizes the gap in the density of conducting states, a gap that is smeared out when the disorder is increased.

In the computation, the energies of those terminal dots that represent the electrodes are not allowed to fluctuate. The energies of the other dots are chosen, as in earlier computations, from a random distribution of a specified range that is centered about the mean energy α_0. The coupling of the electrodes to the other dots is taken to be independent of the compression of the array. The transmission is computed as a function of the energy E_μ of the molecular orbital (above the HOMO, which is nearly but not exactly at α_0). It is then averaged explicitly over a thermal distribution for the unoccupied molecular orbitals. For the temperature range of interest here, i.e., below 300 K, it means that only very low lying excited states will contribute. It is for this reason that the low-temperature conductivity offers such a sensitive probe for the states just above the Fermi energy of the array.

Figure 6 shows the computed transmission as a function of energy E_μ of the molecular orbital. It is intentionally plotted also for states below the Fermi energy in order to show the gap in the density of conducting states, a gap that, in the absence of disorder, occurs at the energy of the HOMO. More on this in section 6 below. When there is a finite but limited disorder, the gap persists, but it narrows in width and is fully bridged at sufficiently high disorder.

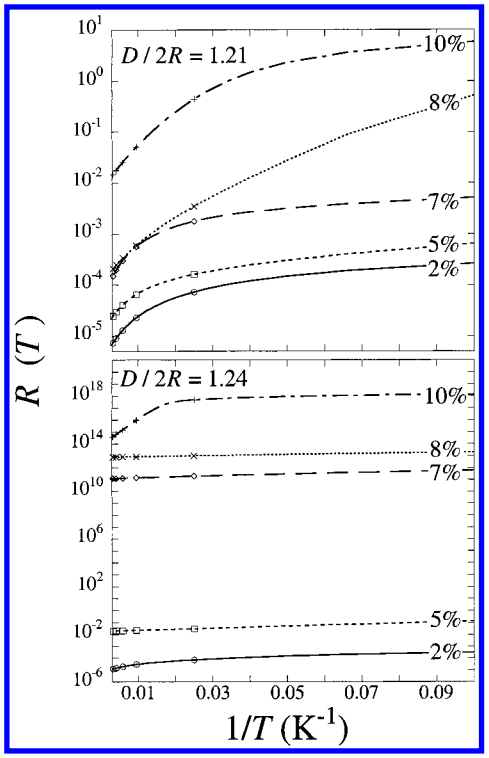

Figure 7. Quantum mechanical computations of the temperature dependence of the resistivity, logarithmic scale, vs $1/T$. Shown for two values of $D/2R$ to emphasize that compressing the array exponentially decreases the resistivity at higher values of disorder but that the resistivity saturates when the states of the array are delocalized. The activated regime where $\ln(R)$ scales as E_a/kT is to the left. At very low temperatures, the dependence is $\ln(R) \propto (E_0/kT)^{1/2}$ as emphasized in Figure 8.

We emphasize that the gap in the density of conducting states and the smearing out of the gap at high disorder are not artifacts of the one-electron approximation. The gap is due to mixed states that congregate above the Fermi energy as already seen in Figures 3 and 4. In fact, it is easy to visualize these states in a Hubbard-like model. In this picture, ionic (*N*-electron) states that can conduct lie higher up in energy because they are penalized by the energetic cost of the Coulombic repulsion of two electrons on the same site. However, if disorder is high enough, this need not be the case. The reason is that it may be energetically advantageous to move an electron from a dot with a high site energy α to another dot, already occupied, but with a lower site energy. Indeed, we have already shown[7] that for higher disorder this effect may be so extreme as to make the (*N*-electron) ground-state ionic, and some evidence of this state has been observed experimentally.[24]

5. The Temperature Dependence of the Conductivity

Averaging the transmission over a thermal distribution of the states of the array provides the conductivity and hence the resistivity, $R(T)$, as a function of temperature. Typical results are plotted vs $1/T$ in Figure 7. The plots exhibit the trends seen in the experimental results:

(a) There is a steep decrease in resistivity with decreasing disorder until one reaches the fully delocalized states.

(b) There is a steep decrease in resistivity with increasing lattice compression until one reaches the fully delocalized states.

Both of these observations are consistent with the view that for the experimental range of low but finite disorder (14−6%[4]) we are in the regime to the right of the transition to a delocalized state.

(c) As a function of temperature, below room temperature, (below ∼200 K in the experiments), there is an activated regime where ln R varies as $1/T$, but at even lower temperatures, there is a crossover to a different regime. We discuss these two mechanisms in sections 7 and 8.

Not seen in the computation is the transition to ordinary metallic conduction, which is experimentally observed at temperatures above about 200 K. This is as it should be. We do not include scattering by phonons, and so this additional contribution to the resistivity is absent in the computations.

6. The Gap in the Density of Conducting States

The transmission as a function of energy shows a cusp-like behavior near the Fermi energy. We shall attribute the variation of the conductivity at very low temperatures to this cusp. This cusp is quite evident in our computations even in the absence of disorder, and it closes in as disorder is increased. As a check of the computations, we now consider a simple model, namely, a linear chain of N quantum dots. A linear chain is not stable against distortions and has other shortcomings as a model. All that we mean to demonstrate here is that the gap in the density of conducting states, as seen in our computations for packing and size disordered hexagonal arrays, can be seen analytically in this toy model. Furthermore, the model shows that the functional form $\exp(-E_0/E)$ fits the behavior of the density of conducting states, where E is the energy measured with respect to the HOMO.

For the model, the sites of the array are enumerated from 1 to N. The two end sites, $j = 1$ and $j' = N$ are coupled to the sites $k = 2$ and $k' = N - 1$, respectively. Hence, in the site basis, the scattering matrix is given by $T_{if} = \langle 1|VGV|N\rangle = V^2\langle 2|G|N-1\rangle$ where V is the coupling of the leads to the rest of the chain, and they are coupled only to their next neighbors. G is the Green's function of the entire chain, including the coupling V. Using the spectral representation of the Green's function in terms of the molecular orbitals of the chain and taking the imaginary part, we have for any state μ of the chain

$$T_{if} = i\pi V^2\langle 2|\delta(E-H)|N-1\rangle = i\pi V^2 \sum_{\mu\ \mathrm{unocc}} C_{2,\mu}C_{N-1,\mu}\delta(E-E_\mu) \quad (13)$$

Here $C_{n,\mu}$ is the amplitude of site orbital n in the molecular orbital μ and the sum is only over the unoccupied molecular orbitals. It is clear that the T matrix element is a weighted density of states. The analytical expressions of the coefficients $C_{n,\mu}$ in eq 13 are $C_{n,\mu} = [2/(N+1)]\sin(n\mu\pi/(N+1))$, $E_\mu = 2\beta\cos(\mu\pi/(N+1))$ and the reduced variable, x, is given by $x = E_\mu/2\beta$, so that $T \propto [2/(N+1)]\sin(2\cos^{-1}x)\sin((N-1)\cos^{-1}x)$. Different states of the chain differ in the value of x, and the transmission for a given state is $|T|^2$. Analytically or numerically, it is easy to show that the transmission of a long chain (so as to smooth the delta function spikes) plotted vs the energy of the MOs has a cusp-like gap at the HOMO. It is reasonable to expect that this result is not unknown, but we know of no earlier reference. The computations for the full array show a similar gap. The interesting temperature dependence of the conductivity arises from taking the thermal average over this increasing (above the Fermi energy which, for the chain, is at $\mu = N/2$) density of conducting states. We reiterate that the gap begins to close when there is some disorder and that it is fully washed away at high disorder.

7. The Activation Energy for Conduction

Below 200 K, ordered, compressed monolayer (70 Å particles) films exhibit activated transport, such that $\ln R \propto E_a/kT$[4]. This exponential temperature dependence is reproduced by the computations that were reported in section 5. Here we discuss an analytic interpretation of the temperature dependence and relate it to the mean energy of the conducting electrons. This result is motivated by the, so-called, Tolman interpretation of the activation energy of chemical reactions.[27] The present result will be somewhat different because of the quantity that is being measured. The reaction rate constant in chemical kinetics is defined as the reaction rate per concentration of the reactants. For the case of the current, if there are more ways of conducting, the currents add up to a limit of the quantum unit of current per state. When there are more charge carriers, there is a higher current. Therefore, in expression 4 for the thermally averaged conductivity, $\langle n_i\rangle$ is the number of carriers in state i without normalization so that, measuring energy with respect to the Fermi level ≡ HOMO

$$\partial\langle n_i\rangle/\partial(1/T) = -((E_i - E_F)/k)\langle n_i\rangle \quad (14)$$

Then we have from eq 4 that neglecting the contribution from the electrodes

$$E_a \equiv -k\partial\ \mathrm{ln}i/\partial(1/T) \equiv -(\partial i/\partial(1/kT))/i = \sum_i(E_i - E_F)\langle n_i\rangle T_i/\sum_i\langle n_i\rangle T_i \quad (15)$$

Remembering that the summation over i is only over states above the Fermi level, we see that E_a, defined as the logarithmic derivative with respect $1/T$, is the mean energy of the conducting electrons.

The experimental observation is that at a lower temperature it makes sense to examine the logarithmic derivative with respect to $1/\sqrt{T}$. Using $\partial\langle n_i\rangle/\partial[1/(T)^{1/2}] = [2/(T)^{1/2}]\partial\langle n_i\rangle/\partial(1/T)$, we find that

$$\sqrt{E_0} \equiv -\frac{1}{2}\sqrt{k}\partial\ \mathrm{ln}i/\partial(1/\sqrt{T}) = \sum_i((E_i - E_F)/\sqrt{kT})\langle n_i\rangle T_i/\sum_i\langle n_i\rangle T_i \quad (16)$$

The parameters E_a and E_0 defined by eqs 15 and 16 are not necessarily constant and can depend on temperature. That the two parameters cannot, in the same range, be both temperature independent is shown by the exact relation $E_0 = E_a^2/kT$. In the remaining part of this section, we argue that at lowest temperatures it is E_0 rather than E_a that is constant. At somewhat higher temperatures, it is E_a that becomes temperature independent, and the cross-over temperature between the two regimes is where the two constants are related.

Our proposed interpretation of the temperature dependence is that it reflects the envelope of the density of the conducting states. This density, when smoothed over the dense spikes of individual molecular orbitals, increases above the Fermi energy as $\exp(-E_0/E)$, where E is the energy measured with respect to the Fermi energy. This increase is over a relatively flat background which is evident in Figure 6. The thermal averaging of this envelope requires multiplying it by the Boltzmann factor for states above the HOMO, $\exp(-E/kT)$, and integrating over E. The integral can be done analytically, but the same result can be obtained by a saddle point approximation, because, at

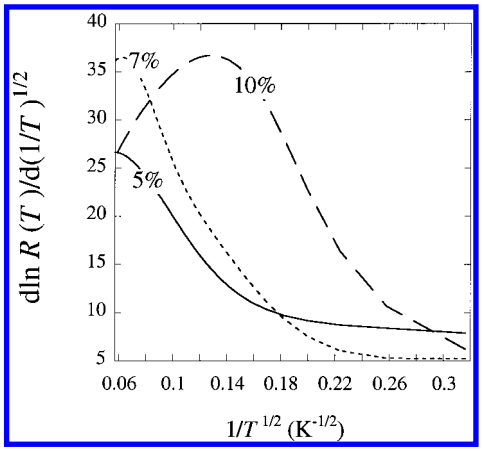

Figure 8. Quantum mechanical computations of the temperature dependence of the resistivity, plotted to emphasize the behavior at lower temperatures where $\ln(R) \propto (E_0/kT)^{1/2}$. Shown is the (analytically computed) logarithmic derivative of $R(T)$ with respect to $T^{-1/2}$ plotted vs $T^{-1/2}$. At low temperatures, this logarithmic derivative is constant and E_0 scales as $\beta^2/\Delta\alpha$. At somewhat higher temperatures, there is a cross over to an activated regime. The dependence of the derivative in the cross over regime is further discussed in section 8 and in Figure 10 below.

energies just above E_F, the integrand is a product of a sharply increasing function, the transmission, Figure 6, and a sharply decreasing function, the Boltzmann weight. The saddle point at the temperature T is the energy $E(T)$ which is the solution of $\partial(-E_0/E - E/kT)/\partial E = 0$. This gives $(E_0/E(T)) = (E_0/kT)^{1/2}$ and shows that the exponential dependence of the conductivity at the low-temperature regime is

$$i \propto \exp(-2(E_0/kT)^{1/2}) \qquad \text{low temperature} \qquad (17)$$

The restriction to low temperature is that at higher energies the density of conducting states levels off, and so one gets the usual activated regime, reflecting a density of conducting states whose envelope is roughly constant.

The energy E_0 is determined by the energies of the orbitals just above the HOMO. In the presence of disorder, this allows for variable range hopping, VRH.[21,26,28] VRH is a term of solid-state physics [28] and is typically interpreted therein in terms of charging energy. By VRH in a one electron picture, we understand what chemists know as super-exchange.[8,14,29] To see this, consider two dots with roughly comparable values of their site energy α. These dots are, however, not adjacent to one another but are separated by another dot with a significantly different site energy. When the exchange coupling is not strong, it cannot couple a dot to its neighbor because the difference, $\Delta\alpha$, in the site energies is too large compared to the coupling. However, the electron can still hop two dots away because now the difference in site energies is smaller. Perturbation theory suggests that the coupling constant is then $\beta^2/\Delta\alpha$.

The computational results for the derivative of the resistivity at low temperatures, Figure 8, do show that E_0 does scale with $\beta^2/\Delta\alpha$. We emphasize that the logarithmic derivative is computed analytically, as in eq 15, and not numerically. The reason we mention it is that the coefficient of proportionality between E_0 and $\beta^2/\Delta\alpha$ does depend on the random drawing of the site energies of the dots. This residual dependence remains even though we have computed using hexagonal arrays of 55 dots per side and 8911 dots in all. Even for such large arrays, there are few enough disorder-induced states in the gap that the scale parameter E_0 is not strictly independent of the specific distribution of dot energies. It is an open question whether this is the same effect as the experimental observation that there appears to be some scatter in the value of E_0 that is determined by measuring the conductivity for different films.

To conclude, the computed value of E_0 scales as $\beta^2/\Delta\alpha$ where $\Delta\alpha$ is a measure of the variance of the site energies. The magnitude of E_0 (for the range of parameters to the right of the transition to the delocalized states it is typically below 1 eV) is in the same range as was observed,[4] but it is somewhat sensitive to higher moments of the size distribution. This is not unexpected because the theory of domain localized regime[8] tells us that variable range coupling should scale with the variance of β^2/α (which is not the same as (β^2/variance of α) = $\beta^2/\Delta\alpha$).

At temperatures above a few tens of degrees, the computations (and the experiment[4]) show a cross-over to an activated regime where the current increases exponentially with temperature as $\exp(-E_a/kT)$. The computed activation energy E_a increases with increasing lattice compression, Figure 7, as is to be expected from the strong dependence of the exchange coupling β on the lattice parameter $D/2R$, cf. Figure 1.

Above around 200 K, the experimental results[4] are that there is an onset of a regime where films reflect as a metal and the resistivity begins to increase with temperature. This is to be physically expected. Our considerations show that as the temperature increases so does the excess energy of the conducting electrons. Unlike the very lowest unoccupied states, these higher energy states can lose energy by inelastic scattering with the phonons, thereby decreasing the conductivity. This effect is not allowed for in the computations, and these therefore cannot and do not reproduce it. The computed resistivity continues to decrease with increasing temperature. Inelastic scattering by the phonons is the familiar loss mechanism for ordered metals. Its onset is well below room temperature. Here, however, the usual disorder-induced density of states precludes its contribution at the lowest temperatures. The reason, as discussed above, is that the very lowest conducting states above the Fermi level are sparse and are domain localized, cf. Figures 2 and 5. These are the states that allow for conductivity at the lowest measured temperatures.

8. The Coexistence Regime

A simple kinetic scheme that accounts for the observed or computed trends of the resistivity with temperature is to assume that the VRH and activated regimes coexist. At the same time, the scheme shows that for realistic values (observed or computed) of the parameters, there is a rapid switch from one mode to another so that, over most of the low temperature range, one mode dominates. The transition regime spans only a narrow temperature range.

The (smoothed) density of conducting states has two contributions, a smooth background and a gap that is closing as the energy increases. When there are two conduction routes, the current will be the sum, and so the resistivity has the form

$$\frac{1}{R} = \frac{1}{R_{VRH}} + \frac{1}{R_a} \propto A_{VRH} \exp(-2(E_0/kT)^{1/2}) + A_a \exp(-E_a/kT) \qquad (18)$$

where the two currents are approximated by their exponential temperature dependence. This equation is plotted in Figure 9 on a logarithmic scale vs $1/T$, for realistic values of the parameters for the case when the two preexponential factors are equal. The result not only mimics well the observed or quantum mechanically computed such plots but also reproduces

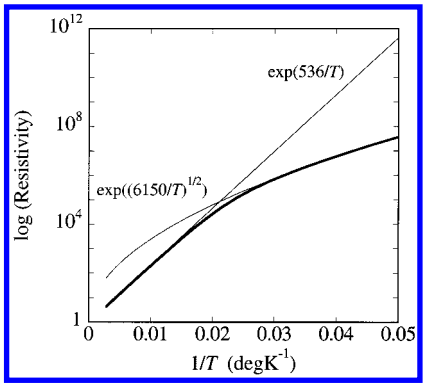

Figure 9. A simple model that reproduces the trends in the temperature dependence of the resistivity (heavy line) as seen in the experiment or in the quantum mechanical computations. The model assumes that two mechanisms are operative at all temperatures, an activated route, where $\ln(R)$ scales as E_a/kT and a variable range hopping (or super-exchange coupling) where $\ln(R) \propto (E_0/kT)^{1/2}$. The resistivity of either mechanism is shown as a light line. Using realistic values for the two energy scales, E_a and E_0, as shown on the plot, the model predicts a rather rapid transition from one regime to another, as the temperature is varied.

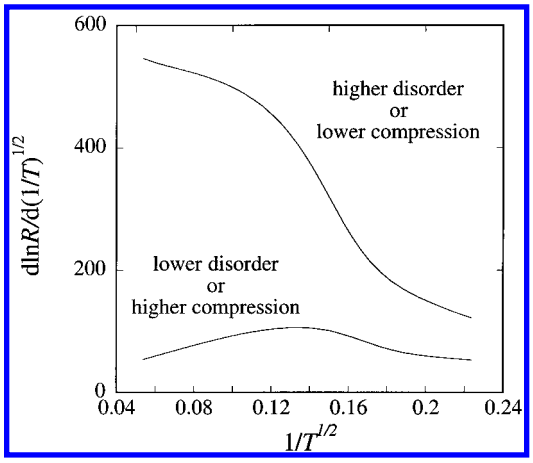

Figure 10. Logarithmic derivative of $R(T)$ with respect to $T^{-1/2}$, computed from the model described in Figure 9 and plotted vs $T^{-1/2}$. The model reproduces the trends seen in the quantum mechanical computations as shown in Figure 8. The experimental results, which can be obtained only when the resistivity is lower, are similar to the curve labeled "lower disorder or higher compression".

the shape of the computed logarithmic derivative of the resistivity with respect temperature.

The transition temperature T_c between the two regimes for the resistivity depends also on the two preexponential factors in eq 18. When the two are equally important, the crossing temperature is the solution of $2(E_0/kT)^{1/2}) = E_a/kT$. This leads to

$$kT_c = (E_a^2/2E_0) \propto (E_a/\beta)^2(\Delta\alpha + \text{constant}) \qquad (19)$$

One knows that there is a constant that remains finite even if there is no disorder because the experiment and the exact computations show that E_0 increases as the disorder decreases. The experimental result is that the crossing temperature does scale linearly with $\Delta\alpha$. When the experimental values of T_c are extrapolated to very low values of $\Delta\alpha$, T_c is found to vanish already for a finite value of $\Delta\alpha$.[4] This is not consistent with eq 19 where T_c remains finite. However, for the compression range sampled in the experiments and for the range of disorder that was accessible, $\Delta\alpha > 6\%$, one is in the domain-localized regime, to the right of the transition to the delocalized state, as shown in Figure 2. Once one allows $\Delta\alpha$ to decrease to very low values, and for any compression, there will come a point when the transition to delocalized states takes place. This is seen in the computations for the lowest values of disorder that are reported in Figure 7. These computations suggest that this is the transition seen in the extrapolation of the experimental results to very low disorder. The final confirmation must await the synthesis of dots with a very narrow size distribution and/or the packing of dots into a more compressed lattice. One can speculate that the geometrical collapse of the hexagonal lattice which is seen experimentally when one tries to compress an array of dots with a small but finite size fluctuation past, say, $D/2R = 1.1$ is related to this phase transition taking place.

The scheme also reproduces well the features of the quantum mechanically computed logarithmic derivative of the resistivity as shown in Figure 10. The characteristic peak in the derivative as seen in the exact computations for higher disorder and/or lower compression, cf. Figure 8, is well reproduced. The parameters E_a and E_0 in Figures 9 and 10 (E_a of the order of 500 K and E_0 between 7000 and 3000 K as a strongly decreasing function of increasing disorder) are consistent with both experimental and quantum mechanical computational results for the range of parameters probed in the experiment. The quantum mechanical results can and have been extended to lower values of disorder where one sees a transition to conduction by delocalized states.

9. Concluding Remarks

An interpretation of experimental and quantum mechanical computations of the temperature-dependent conductivity of arrays of quantum dots has been proposed. It is suggested that the experiment spans the regime just before the transition to a conducting, electronically delocalized state of the array. In this regime, the electronic states just above the Fermi level are domain-localized,[8] and the conductivity at the lowest temperature is determined by the electrons hopping not necessarily between adjacent dots, a so-called variable range hopping.[21,28] The exchange coupling of adjacent dots leads, in this disorder-induced regime, to super exchange[29] coupling of more distant dots. The characteristic energy scale of this regime is higher for arrays of lower disorder. Below room temperatures, the conductivity is dominated by higher energy excited states of the array and so shows the familiar activated temperature dependence. The activation energy was shown to be the mean energy of the conducting electrons. The transition between the two regimes is sensitive to the amount of disorder.

The results show that measuring the temperature dependence of the conductivity provides a very high resolution probe of the lower lying excited states of the array. Theory suggests that there is further scope that can be uncovered using dots of even narrower size distribution and/or more compressed arrays and higher voltages where the response is no longer linear. There are significant experimental problems in realizing these goals, but theory suggests that the effort will be worthwhile. At the other end, when the size distribution of the dots becomes wider and or the lattice is not quite compressed, theory shows, cf. Figure 7, an exponentially decreasing conductivity because of the cross over to an electronically localized regime. This cannot be probed in the same dynamic range as the conductivity of the packed films with a narrow size variation of the dots. It will however be worthwhile to experimentally document the transition from the localized to the domain-localized regime. This transition and the effect of voltage have already been seen[9] in the coarser measurements of the surface potential, and the correspondence therein between experiment and theory suggests

that temperature-dependent measurements of the surface potential and of the conductivity, for a wider range of conditions, should be carried out.

Acknowledgment. This work was funded by the Department of Energy and by a CULAR grant. F.R. is a "Maître de Recherche", FNRS, Belgium and thanks Liège University for a "Crédit d'impulsion" grant. This work used the computational facilities provided by SFB 377 (Hebrew University) and NIC (Liège University).

References and Notes

(1) Chen, J.; Reed, M. A.; Rawlett, A. M.; Tour, J. M. *Science* **1999**, *286*, 1550. Collier, C. P.; Mattersteig, G.; Wong, E. W.; Luo, Y.; Beverly, K.; Sampaio, J.; Raymo, F. M.; Stoddart, J. F.; Heath, J. R. *Science* **2000**, *289*, 1172. Ellenbogen, J. C.; Love, J. C. *Proc. IEEE* **2000**, *88*, 386. Joachim, C.; Gimzewski, J. K.; Aviram, A. *Nature* **2000**, *408*, 541. Metzger, R. M. *Acc. Chem. Res.* **1999**, *32*, 950. Postma, H. W. C.; Teepen, T.; Yao, Z.; Grifoni, M.; Dekker, C. *Science* **2001**, *293*, 76. Rueckes, T.; Kim, K.; Joselevich, E.; Tseng, G. Y.; Cheung, C. L.; Lieber, C. M. *Science* **2000**, *289*, 94. Bachtold, A.; Fuhrer, M. S.; Plyasunov, S.; Forero, M.; Anderson, E. H.; Zettl, A.; McEuen, P. L. *Phys. Rev. Lett.* **2000**, *84*, 6082.

(2) Andres, R. P.; Bein, T.; Dorogi, M.; Feng, S.; Henderson, J. I.; Kubiak, C. P.; Mahoney, W.; Osifchin, R. G.; Reifenberger, R. *Science* **1996**, *272*, 1323. Kim, S. H.; Markovich, G.; Rezvani, S.; Choi, S. H.; Wang, K. L.; Heath, J. R. *Appl. Phys. Lett.* **1999**, *74*, 317. Black, C. T.; Murray, C. B.; Sandstrom, R. L.; Sun, S. H. *Science* **2000**, *290*, 1131. Lin, X. M.; Jaeger, H. M.; Sorensen, C. M.; Klabunde, K. J. *J. Phys. Chem.* **2001**, *105*, 3353. Sampaio, J. F., Beverly, K. C., Heath, J. R. *J. Phys. Chem. B* **2001**, *105*, 8797. Doty, R. C.; Yu, H. B.; Shih, C. K.; Korgel, B. A. *J. Phys. Chem. B* **2001**, *105*, 8291. Quinn, B. M.; Prieto, I.; Haram, S. K.; Bard, A. J. *J. Phys. Chem. B* **2001**, *105*, 7474.

(3) Kubo, R. *J. Phys. Soc. Jpn.* **1962**, *17*, 975. Reed, M. *Sci. Am.* **1993**, *268*, 98. Ashoori, R. C. *Nature* **1996**, *379*, 413.

(4) Beverly, K. C.; Sampaio, J. F.; Heath, J. R. *J. Phys. Chem. B* **2002**, *106*, 2131.

(5) Remacle, F.; Collier, C. P.; Heath, J. R.; Levine, R. D. *Chem. Phys. Lett.* **1998**, *291*, 453.

(6) Remacle, F.; Levine, R. D. *J. Am. Chem. Soc.* **2000**, *122*, 4084.

(7) Remacle, F.; Levine, R. D. *J. Phys. Chem. A* **2000**, *104*, 10435.

(8) Remacle, F.; Levine, R. D. *J. Phys. Chem. B* **2001**, *105*, 2153.

(9) Sample, J. L.; Beverly, K. C.; Chaudhari, P. R.; Remacle, F.; Heath, J. R.; Levine, R. D. *Adv. Mater.* **2002**, *114*, 124.

(10) Imry, Y.; Landauer, R. *Rev. Mod. Phys.* **1999**, *71*, S306.

(11) Datta, S. *Electronic Transport in Mesoscopic Systems*; Cambridge University Press: Cambridge, U.K., 1995.

(12) Mujica, V.; Kemp, M.; Ratner, M. A. *J. Chem. Phys* **1994**, *101*, 6849.

(13) Yaliraki, S. N.; Ratner, M. A. *J. Chem. Phys.* **1998**, *109*, 5036. Xue, Y.; Datta, S.; Ratner, M. A. *J. Chem. Phys.* **2001**, *115*, 4292. Samanta, M. P.; Tian, W.; Datta, S.; Henderson, J. I.; Kubiak, C. P. *Phys. Rev. B* **1996**, *53*, R7626. Tian, W. D.; Datta, S.; Hong, S. H.; Reifenberger, R.; Henderson, J. I.; Kubiak, C. P. *J. Chem. Phys* **1998**, *109*, 2874.

(14) Hsu, C. P.; Marcus, R. A. *J. Chem. Phys.* **1997**, *106*, 584.

(15) Remacle, F.; Levine, R. D. *J. Phys. Chem. A* **2000**, *104*, 2341.

(16) Middleton, A. A.; Wingreen, N. S. *Phys. Rev. Lett.* **1993**, *71*, 3198.

(17) Levine, R. D. *Quantum Mechanics of Molecular Rate Processes*; Dover: New York, 1999.

(18) Remacle, F.; Levine, R. D. *Proc. Natl. Acad. Sci. U.S.A.* **2000**, *97*, 553.

(19) Remacle, F.; Levine, R. D. *ChemPhysChem* **2001**, *2*, 20.

(20) Hubbard, J. *Proc. R. Soc.* **1963**, *276*, 238.

(21) Mott, N. F. *Metal−Insulator Transitions*; Taylor & Francis: London, 1990.

(22) Schatz, G. C.; Ratner, M. A. *Quantum Mechanics in Chemistry*; Prentice Hall: New York, 1993.

(23) Henrichs, S.; Collier, C. P.; Saykally, R. J.; Shen, Y. R.; Heath, J. R. *J. Am. Chem. Soc.* **2000**, *122*, 4077.

(24) Kim, S. H.; Medeiros-Ribeiro, G.; Ohlberg, D. A. A.; Williams, R. S.; Heath, J. R. *J. Phys. Chem B* **1999**, *103*, 10341.

(25) Remacle, F.; Collier, C. P.; Markovitch, G.; Heath, J. R.; Banin, U.; Levine, R. D. *J. Phys. Chem. B* **1998**, *102*, 7727.

(26) Zallen, R. *The Physics of Amorphous Solids*; Wiley: New York, 1983.

(27) Tolman, R. C. *The Principles of Statistical Mechanics*; Dover: New York, 1979.

(28) Shklovskii, B. I.; Efros, A. L. *Electronic Properties of Doped Semiconductors*; Springer-Verlag: Berlin, Germany, 1984.

(29) McConnell, H. M. *J. Chem. Phys.* **1961**, *35*, 508.